Estimating temporally variable selection intensity from ancient DNA data with the flexibility of modelling linkage and epistasis

Zhangyi He[a,1,*], Xiaoyang Dai[b,1], Wenyang Lyu[c], Mark Beaumont[d], Feng Yu[c]

[a] *Cancer Research UK Beatson Institute, Glasgow G61 1BD, United Kingdom*
[b] *The Blizard Institute, Barts and The London School of Medicine and Dentistry, Queen Mary University of London, London E1 2AT, United Kingdom*
[c] *School of Mathematics, University of Bristol, Bristol BS8 1UG, United Kingdom*
[d] *School of Biological Sciences, University of Bristol, Bristol BS8 1TQ, United Kingdom*

Abstract

Innovations in ancient DNA (aDNA) preparation and sequencing technologies have exponentially increased the quality and quantity of aDNA data extracted from ancient biological materials. The additional temporal component from the incoming aDNA data can provide improved power to address fundamental evolutionary questions like characterising selection processes that shape the phenotypes and genotypes of contemporary populations or species. However, utilising aDNA to study past selection processes still involves considerable hurdles such as how to eliminate the confounding effect of genetic interactions in the inference of selection. To circumvent this challenge, in this work we extend the method introduced by He et al. (2022) to infer temporally variable selection from the data on aDNA sequences with the flexibility of modelling linkage and epistasis. Our posterior computation is carried out through a robust adaptive version of the particle marginal Metropolis-Hastings algorithm with a coerced acceptance rate. Moreover, our extension inherits their desirable features like modelling sample uncertainties resulting from the damage and fragmentation of aDNA molecules and reconstructing underlying gamete frequency trajectories of the population. We assess the performance and show the utility of our procedure with an application to ancient horse samples genotyped at the loci encoding base coat colours and pinto coat patterns.

Keywords: Ancient DNA, Natural selection, Genetic linkage, Epistatic interaction, Two-layer hidden Markov model, Adaptive particle marginal Metropolis-Hastings

*Corresponding author.
Email address: z.he@beatson.gla.ac.uk (Zhangyi He)
[1] These authors contributed equally to this work.

1. Introduction

Natural selection is one of the primary mechanisms of evolutionary changes and is responsible for the evolution of adaptive features (Darwin, 1859). A full understanding of the role of selection in driving evolutionary changes needs accurate estimates of the underlying timing and strength of selection. With recent advances in sequencing technologies and molecular techniques tailored to ultra-damaged templates, high-quality time serial samples of segregating alleles have become increasingly common in ancestral populations, (*e.g.*, Mathieson et al., 2015; Loog et al., 2017; Fages et al., 2019; Alves et al., 2019). The additional temporal dimension of the ancient DNA (aDNA) data has the promise of boosting power of estimating population genetic parameters, in particular for the pace of adaptation, as the allele frequency trajectory through time itself gives us valuable information collected before, during and after genetic changes driven by selection. See Dehasque et al. (2020) for a detailed review of the inference of selection from aDNA.

The temporal component provided by the incoming aDNA data spurred the development of statistical approaches for the inference of selection from time series data of allele frequencies in the last fifteen years (see Malaspinas, 2016, for a detailed review). Most existing approaches are built upon the hidden Markov model (HMM) framework of Williamson & Slatkin (1999), where the population allele frequency is modelled as a hidden state evolving under the Wright-Fisher model (Fisher, 1922; Wright, 1931), and the sample allele frequency drawn from the underlying population at each given time point is modelled as a noisy observation of the population allele frequency (see Tataru et al., 2017, for an excellent review of statistical inference in the Wright-Fisher model based on time series data of allele frequencies). However, such an HMM framework can be computationally infeasible for large population sizes and evolutionary timescales owing to a prohibitively large amount of computation and storage required in its likelihood calculations.

To our knowledge, most existing methods tailored to aDNA depend on the diffusion limit of the Wright-Fisher model. By working with the diffusion limit, its HMM framework permits efficient integration over the probability distribution of the underlying population allele frequencies and hence the calculation of the likelihood based on the observed sample allele frequencies can be completed within a reasonable amount of time (*e.g.*, Bollback et al., 2008; Malaspinas et al., 2012; Steinrücken et al., 2014; Schraiber et al., 2016; Ferrer-Admetlla et al., 2016; He et al., 2020b,c; Lyu et al., 2022; He et al., 2022). These approaches have been successfully applied in

aDNA studies, *e.g.*, the method of Bollback et al. (2008) was used in Ludwig et al. (2009) to analyse the aDNA data associated with horse coat colouration and showed that positive selection acted on the derived *ASIP* and *MC1R* alleles, suggesting that domestication and selective breeding contributed to changes in horse coat colouration.

Despite the availability of a certain number of statistical methods for the inference of selection from genetic time series, their application to aDNA data from natural populations remains limited. Most existing methods were developed in the absence of genetic interactions like linkage and epistasis, with the exception of *e.g.*, He et al. (2020b). In He et al. (2020b), local linkage and genetic recombination were explicitly modelled, which has been demonstrated to contribute to significant improvements in the inference of selection, in particular for tightly linked loci. Ignoring epistasis can also cause severe issues in the study of selection since the combined effects of mutant alleles may be impossible to predict according to the measured individual effects of a given mutant allele (Bank et al., 2014). As an example, horse base coat colours (*i.e.*, bay, black and chestnut) are primarily determined by *ASIP* and *MC1R*, and the derived *ASIP* and *MC1R* alleles have been shown to be selectively advantageous with ancient horse samples through existing approaches (*e.g.*, Bollback et al., 2008; Malaspinas et al., 2012; Steinrücken et al., 2014; Schraiber et al., 2016; He et al., 2020c). However, this is not sufficient enough to conclude that black horses were favoured by selection as alleles at *MC1R* interact epistatically with those at *ASIP*, *i.e.*, the presence of at least one copy of the dominant ancestral allele at *MC1R*, and the resulting production of black pigment, is required to check the action of alleles at *ASIP* (Corbin et al., 2020).

To circumvent this issue, in this work we introduce a novel Bayesian method for the inference of selection acting on the phenotypic trait, allowing the intensity to vary over time, from data on aDNA sequences, with the flexibility of modelling genetic linkage and epistatic interaction. Our method is built upon the two-layer HMM framework of He et al. (2022), and our key innovation is to introduce a Wright-Fisher diffusion that can model the dynamics of two linked genes under phenotypic selection over time to be the underlying Markov process, which permits linkage and epistasis. To remain computationally feasible, our posterior computation is carried out with the particle marginal Metropolis-Hastings (PMMH) algorithm introduced by Andrieu et al. (2010), where we adopt the adaption strategy proposed by Vihola (2012) to tune the covariance structure

of the proposal to achieve a given acceptance rate. Also, our approach inherits certain desirable features from He et al. (2022) like modelling sample uncertainties resulting from the damage and fragmentation of aDNA molecules and reconstructing underlying frequency trajectories of the gametes in the population.

We reanalyse the aDNA data associated with horse base coat colours and pinto coat patterns from Wutke et al. (2016) to show the applicability of our method on aDNA data, where base coat colours (bay, black and chestnut) are controlled by the *ASIP* and *MC1R* genes with epistatic interaction while pinto coat patterns (solid, sabino and tobiano) are determined by the *KIT13* and *KIT16* genes with tight linkage. We compare our results with those produced through the approach of He et al. (2022) to demonstrate the necessity of modelling linkage and epistasis in the inference of selection. We test our approach with extensive simulations for each phenotypic trait to show that our procedure can deliver accurate selection inferences from genotype likelihoods.

2. Materials and Methods

In this section, we construct a Wright-Fisher model to characterise two linked genes evolving under phenotypic selection over time first and then derive its diffusion limit. Working with the diffusion approximation, we extend the approach of He et al. (2022) to infer temporally variable selection from the data on aDNA sequences while modelling linkage and epistasis.

2.1. Wright-Fisher diffusion

We consider a population of randomly mating diploid individuals represented by alleles at loci $\mathcal{A}$ and $\mathcal{B}$ evolving under selection with discrete non-overlapping generations. At each locus, there are two possible allele types, labelled $\mathcal{A}_0$, $\mathcal{A}_1$ and $\mathcal{B}_0$, $\mathcal{B}_1$, respectively, resulting in four possible haplotypes on both loci, $\mathcal{A}_0\mathcal{B}_0$, $\mathcal{A}_0\mathcal{B}_1$, $\mathcal{A}_1\mathcal{B}_0$ and $\mathcal{A}_1\mathcal{B}_1$, labelled haplotypes 00, 01, 10 and 11, respectively. We attach the symbols $\mathcal{A}_0$ and $\mathcal{B}_0$ to the ancestral alleles, which we assume originally exist in the population, and we attach the symbols $\mathcal{A}_1$ and $\mathcal{B}_1$ to the mutant alleles, which we assume arise only once in the population. Given the absence of sex effects, this setup gives rise to 10 possible (unordered) genotypes $\mathcal{A}_i\mathcal{B}_j/\mathcal{A}_{i'}\mathcal{B}_{j'}$, which correspond to at most 10 distinct phenotypes $\mathcal{P}_{ij,i'j'}$. Phenotypes $\mathcal{P}_{ij,i'j'}$ and $\mathcal{P}_{i'j',ij}$ are identical in our notation.

We incorporate viability selection into the population dynamics and assume that the viability is only determined by the phenotype. Viabilities of all genotypes at loci $\mathcal{A}$ and $\mathcal{B}$ per generation

are assigned $1 + s_{ij,i'j'}$, where $s_{ij,i'j'}$ is the selection coefficient of the $\mathcal{P}_{ij,i'j'}$ phenotype with $s_{ij,i'j'} \in [-1, +\infty)$ and $s_{ij,i'j'} = s_{i'j',ij}$. In what follows, we let the selection coefficient $s_{00,00} = 0$ unless otherwise noted, and then $s_{ij,i'j'}$ denotes the selection coefficient of the $\mathcal{P}_{ij,i'j'}$ phenotype against the $\mathcal{P}_{00,00}$ phenotype.

2.1.1. Wright-Fisher model

Let $X_{ij}^{(N)}(k)$ denote the gamete frequency of haplotype ij at generation $k \in \mathbb{N}$ and $\boldsymbol{X}^{(N)}(k)$ be the vector of the four gamete frequencies. To incorporate non-constant demographic histories, we assume that the population size changes deterministically, with $N(k)$ denoting the number of diploid individuals in the population at generation k. In the Wright-Fisher model, we assume that gametes are randomly chosen from an effectively infinite gamete pool reflecting the parental gamete frequencies at each generation. We therefore have

$$\boldsymbol{X}^{(N)}(k+1) \mid \boldsymbol{X}^{(N)}(k) = \boldsymbol{x} \sim \frac{1}{2N(k)} \text{Multinomial}(2N(k), \boldsymbol{p}), \tag{1}$$

where $\boldsymbol{p}$ is the vector of parental gamete frequencies. Under the assumption of random mating, we can further express the vector of parental gamete frequencies as

$$p_{ij} = (1-r)x'_{ij} + r(\sum_{j=0}^{1} x'_{ij})(\sum_{i=0}^{1} x'_{ij}) \tag{2}$$

for $i, j \in \{0, 1\}$, where

$$x'_{ij} = \frac{\sum_{i',j'=0}^{1}(1 + s_{ij,i'j'})x_{i'j'}x_{ij}}{\sum_{i,j=0}^{1}\sum_{i',j'=0}^{1}(1 + s_{ij,i'j'})x_{i'j'}x_{ij}},$$

and r denotes the recombination rate of the $\mathcal{A}$ and $\mathcal{B}$ loci located on the same chromosome, *i.e.*, the fraction of recombinant offspring showing a crossover between the two loci per generation. If the $\mathcal{A}$ and $\mathcal{B}$ loci are located on separate chromosomes, we let the (artificial) recombination rate $r = 0.5$ (*i.e.*, free recombination). The two-locus Wright-Fisher model with selection is defined as the Markov process $\boldsymbol{X}^{(N)}$ evolving with transition probabilities in Eq. (1) in the state space $\Omega_{\boldsymbol{X}^{(N)}} = \{\boldsymbol{x} \in \{0, 1/(2N), \ldots, 1\}^4 : \sum_{i,j=0}^{1} x_{ij} = 1\}$.

2.1.2. Diffusion approximation

We study the two-locus Wright-Fisher model with selection through its diffusion limit due to the complicated nature of its transition probability matrix, in particular for large population

sizes or evolutionary timescales. More specifically, we measure time in a unit of $2N_0$ generations, denoted by t, where N_0 is an arbitrary reference population size fixed through time, and assume that the selection coefficients and recombination rate are all of order $1/(2N_0)$. As the reference population size N_0 approaches infinity, the scaled selection coefficients $\alpha_{ij,i'j'} = 2N_0 s_{ij,i'j'}$ and the scaled recombination rate $\rho = 4N_0 r$ are kept constant, and the ratio of the population size to the reference population size $N(t)/N_0$ converges to a function, denoted by $\beta(t)$. Notice that the assumption will be violated if the $\mathcal{A}$ and $\mathcal{B}$ loci are located on separate chromosomes, *i.e.*, $r = 0.5$, but we shall nevertheless use this scaling to find the drift term in the diffusion limit. We will plug the unscaled recombination rate r into the resulting system of stochastic differential equations (SDE's) and use that as our diffusion approximation.

Let $\Delta X_{ij}^{(N)}(k)$ denote the change in the gamete frequency of haplotype ij over generation k. With standard techniques of diffusion theory (see, *e.g.*, Karlin & Taylor, 1981), we can formulate the infinitesimal mean vector $\boldsymbol{\mu}(t, \boldsymbol{x})$ and the infinitesimal (co)variance matrix $\boldsymbol{\Sigma}(t, \boldsymbol{x})$ as

$$\begin{aligned}
\mu_{ij}(t, \boldsymbol{x}) &= \lim_{N_0 \to \infty} 2N_0 \, \mathrm{E}[\Delta X_{ij}^{(N)}([2N_0 t]) \mid \boldsymbol{X}^{(N)}([2N_0 t]) = \boldsymbol{x}] \\
&= \lim_{N_0 \to \infty} 2N_0 (p_{ij} - x_{ij}) \\
\Sigma_{ij,i'j'}(t, \boldsymbol{x}) &= \lim_{N_0 \to \infty} 2N_0 \, \mathrm{E}[\Delta X_{ij}^{(N)}([2N_0 t]) \Delta X_{i'j'}^{(N)}([2N_0 t]) \mid \boldsymbol{X}^{(N)}([2N_0 t]) = \boldsymbol{x}] \\
&= \lim_{N_0 \to \infty} \frac{2N_0}{2N([2N_0 t])} p_{ij}(\delta_{ii'}\delta_{jj'} - p_{i'j'}) + 2N_0 (p_{ij} - x_{ij})(p_{i'j'} - x_{i'j'})
\end{aligned}$$

for $i, j, i', j' \in \{0, 1\}$, where δ denotes the Kronecker delta function and $[\,\cdot\,]$ is used to represent the integer part of the value in the brackets.

To obtain the expression for the infinitesimal mean vector $\boldsymbol{\mu}(t, \boldsymbol{x})$, we compute the limit of the expected change in the gamete frequency of haplotype ij within a single generation as the reference population size N_0 goes to infinity. The only terms that survive after taking the limit are the first order terms in the Taylor expansion of the sampling probability p_{ij} in Eq. (2) with respect to the selection coefficients $s_{ij,i'j'}$ and the recombination rate r. The infinitesimal mean vector $\boldsymbol{\mu}(t, \boldsymbol{x})$ can then be written down as

$$\mu_{ij}(t, \boldsymbol{x}) = x_{ij} \sum_{i',j'=0}^{1} \alpha_{ij,i'j'} x_{i'j'} - x_{ij} \sum_{i',j'=0}^{1} \sum_{i,j=0}^{1} x_{ij} \alpha_{ij,i'j'} x_{i'j'} - (-1)^{\delta_{ij}} \frac{\rho}{2} (x_{00}x_{11} - x_{01}x_{10}) \quad (3)$$

for $i, j \in \{0, 1\}$. Note that we take the scaled recombination rate to be $\rho = 2N_0$ (*i.e.*, the (artificial) recombination rate $r = 0.5$) if the $\mathcal{A}$ and $\mathcal{B}$ loci are located on separate chromosomes. Such a strong recombination term serves to uncouple the two genes located on separate chromosomes. The infinitesimal (co)variance matrix $\boldsymbol{\Sigma}(t, \boldsymbol{x})$ corresponds to the standard Wright-Fisher diffusion on four haplotypes (see, *e.g.*, He et al., 2020a). That is, we have

$$\Sigma_{ij,i'j'}(t, \boldsymbol{x}) = \frac{x_{ij}(\delta_{ii'}\delta_{jj'} - x_{i'j'})}{\beta(t)} \tag{4}$$

for $i, j, i', j' \in \{0, 1\}$.

Combining the Wright-Fisher diffusion with the infinitesimal mean vector $\boldsymbol{\mu}(t, \boldsymbol{x})$ in Eq. (3) and the infinitesimal (co)variance matrix $\boldsymbol{\Sigma}(t, \boldsymbol{x})$ in Eq. (4), we achieve the following system of SDE's as our diffusion approximation of the Wright-Fisher model in Eq. (1)

$$dX_{ij}(t) = \mu_{ij}(t, \boldsymbol{X}(t))dt + \sum_{i',j'=0}^{1} \sqrt{\frac{X_{ij}(t)X_{i'j'}(t)}{\beta(t)}}\, dW_{ij,i'j'}(t) \tag{5}$$

for $i, j \in \{0, 1\}$, where $W_{ij,i'j'}$ denotes an independent standard Wiener process with $W_{ij,i'j'}(t) = -W_{i'j',ij}(t)$. This anti-symmetry requirement implies $W_{ij,ij}(t) = 0$, and the (co)variance matrix for the X_{ij}'s is exactly the infinitesimal (co)variance matrix $\boldsymbol{\Sigma}(t, \boldsymbol{x})$ in Eq. (4). We refer to the diffusion process $\boldsymbol{X}$ evolving in the state space $\Omega_{\boldsymbol{X}} = \{\boldsymbol{x} \in [0, 1]^4 : \sum_{i,j=0}^{1} x_{ij} = 1\}$ that solves the system of SDE's in Eq. (5) as the two-locus Wright-Fisher diffusion with selection.

2.2. Bayesian inference of selection

Suppose that the available data are always sampled from the underlying population at a finite number of distinct time points, say $t_1 < t_2 < \ldots < t_K$, measured in units of $2N_0$ generations. We assume that N_k individuals are drawn from the underlying population at the k-th sampling time point, and for individual n, let $\boldsymbol{r}_{l,n,k}$ be, in this generic notation, all of the reads at locus l for $l \in \{1, 2\}$. The population genetic quantities of our interest are the selection coefficients $s_{ij,i'j'}$ for $i, j, i', j' \in \{0, 1\}$. Recall that our setup gives rise to at most 10 distinct phenotypes (*i.e.*, at most 9 distinct selection coefficients). For simplicity, we use $\boldsymbol{\vartheta}$ to represent all distinct selection coefficients to estimate.

2.2.1. Hidden Markov model

We extend the two-layer HMM framework introduced by He et al. (2022) to model genetic linkage and epistatic interaction, where the first hidden layer $\boldsymbol{X}(t)$ characterises the gamete frequency trajectories of the underlying population over time through the Wright-Fisher diffusion in Eq. (5), the second hidden layer $\boldsymbol{G}(t)$ represents the genotype of the individual in the sample, and the third observed layer $\boldsymbol{R}(t)$ denotes the data on ancient DNA sequences (see Figure 1).

We let $\boldsymbol{x}_{1:K} = \{\boldsymbol{x}_1, \boldsymbol{x}_2, \ldots, \boldsymbol{x}_K\}$ be the frequency trajectories of the gametes in the underlying population at the sampling time points $\boldsymbol{t}_{1:K}$ and $\boldsymbol{g}_{1:K} = \{\boldsymbol{g}_1, \boldsymbol{g}_2, \ldots, \boldsymbol{g}_K\}$ be the genotypes of the individuals drawn from the underlying population at the sampling time points $\boldsymbol{t}_{1:K}$, where $\boldsymbol{g}_k = \{\boldsymbol{g}_{1,k}, \boldsymbol{g}_{2,k}, \ldots, \boldsymbol{g}_{N_k,k}\}$ and $\boldsymbol{g}_{n,k} = \{g_{1,n,k}, g_{2,n,k}\}$ with $g_{l,n,k} \in \{0, 1, 2\}$ being the number of mutant alleles at locus l in individual n at sampling time point t_k. Based on the HMM framework illustrated in Figure 1, the posterior probability distribution for the selection coefficients and population gamete frequency trajectories can be expressed as

$$p(\boldsymbol{\vartheta}, \boldsymbol{x}_{1:K} \mid \boldsymbol{r}_{1:K}) = \sum_{\boldsymbol{g}_{1:K}} p(\boldsymbol{\vartheta}, \boldsymbol{x}_{1:K}, \boldsymbol{g}_{1:K} \mid \boldsymbol{r}_{1:K}),$$

where

$$p(\boldsymbol{\vartheta}, \boldsymbol{x}_{1:K}, \boldsymbol{g}_{1:K} \mid \boldsymbol{r}_{1:K}) \propto p(\boldsymbol{\vartheta}) p(\boldsymbol{x}_{1:K} \mid \boldsymbol{\vartheta}) p(\boldsymbol{g}_{1:K} \mid \boldsymbol{x}_{1:K}) p(\boldsymbol{r}_{1:K} \mid \boldsymbol{g}_{1:K}) \tag{6}$$

and $\boldsymbol{r}_{1:K} = \{\boldsymbol{r}_1, \boldsymbol{r}_2, \ldots, \boldsymbol{r}_K\}$ with $\boldsymbol{r}_k = \{\boldsymbol{r}_{1,k}, \boldsymbol{r}_{2,k}, \ldots, \boldsymbol{r}_{N_k,k}\}$ and $\boldsymbol{r}_{n,k} = \{\boldsymbol{r}_{1,n,k}, \boldsymbol{r}_{2,n,k}\}$.

The first term of the product in Eq. (6), $p(\boldsymbol{\vartheta})$, is the prior probability distribution for the selection coefficients. We can adopt a uniform prior over the interval $[-1, +\infty)$ for each selection coefficient if our prior knowledge is poor.

The second term of the product in Eq. (6), $p(\boldsymbol{x}_{1:K} \mid \boldsymbol{\vartheta})$, is the probability distribution for the population gamete frequency trajectories at all sampling time points. As the Wright-Fisher diffusion is a Markov process, we can decompose the probability distribution $p(\boldsymbol{x}_{1:K} \mid \boldsymbol{\vartheta})$ as

$$p(\boldsymbol{x}_{1:K} \mid \boldsymbol{\vartheta}) = p(\boldsymbol{x}_1 \mid \boldsymbol{\vartheta}) \prod_{k=1}^{K-1} p(\boldsymbol{x}_{k+1} \mid \boldsymbol{x}_k; \boldsymbol{\vartheta}),$$

where $p(x_1 \mid \boldsymbol{\vartheta})$ is the prior probability distribution for the population gamete frequencies at the initial sampling time point, set to be a flat Dirichlet distribution over the state space $\Omega_{\boldsymbol{X}}$ if our

prior knowledge is poor, and $p(\boldsymbol{x}_{k+1} \mid \boldsymbol{x}_k; \boldsymbol{\vartheta})$ is the transition probability density function of the Wright-Fisher diffusion $\boldsymbol{X}$ between two consecutive sampling time points for $k = 1, 2, \ldots, K-1$, solving the Kolmogorov backward equation (or its adjoint) associated with the Wright-Fisher diffusion in Eq. (5).

The third term of the product in Eq. (6), $p(\boldsymbol{g}_{1:K} \mid \boldsymbol{x}_{1:K})$, is the probability distribution for the genotypes of all individuals in the sample given the population gamete frequency trajectories at all sampling time points. With the conditional independence from our HMM framework (see Figure 1), we can decompose the probability distribution $p(\boldsymbol{g}_{1:K} \mid \boldsymbol{x}_{1:K})$ as

$$p(\boldsymbol{g}_{1:K} \mid \boldsymbol{x}_{1:K}) = \prod_{k=1}^{K} p(\boldsymbol{g}_k \mid \boldsymbol{x}_k) = \prod_{k=1}^{K} \prod_{n=1}^{N_k} p(\boldsymbol{g}_{n,k} \mid \boldsymbol{x}_k),$$

where $p(\boldsymbol{g}_{n,k} \mid \boldsymbol{x}_k)$ is the probability distribution for the genotypes $\boldsymbol{g}_{n,k}$ of sampled individual n given the gamete frequencies $\boldsymbol{x}_k$ of the population. Under the assumption that all individuals in the sample are drawn from the population in their adulthood (*i.e.*, the stage after selection but before recombination in the life cycle, see He et al. (2017)), the probability of observing the sampled individual genotypes $\boldsymbol{g}_{n,k} = (i + i', j + j')$ given the population gamete frequencies $\boldsymbol{x}_k$ can be calculated with

$$p(\boldsymbol{g}_{n,k} \mid \boldsymbol{x}_k) = \begin{cases} \dfrac{(1 + s_{ij,i'j'}) x_{i'j',k} x_{ij,k}}{\sum_{i,j=0}^{1} \sum_{i',j'=0}^{1} (1 + s_{ij,i'j'}) x_{i'j',k} x_{ij,k}}, & \text{if } i + i' \neq 1 \text{ and } j + j' \neq 1 \\ \dfrac{(1 + s_{00,11}) 2x_{11,k} x_{00,k} + (1 + s_{01,10}) 2x_{10,k} x_{01,k}}{\sum_{i,j=0}^{1} \sum_{i',j'=0}^{1} (1 + s_{ij,i'j'}) x_{i'j',k} x_{ij,k}}, & \text{if } i + i' = 1 \text{ and } j + j' = 1 \\ \dfrac{(1 + s_{ij,i'j'}) 2x_{i'j',k} x_{ij,k}}{\sum_{i,j=0}^{1} \sum_{i',j'=0}^{1} (1 + s_{ij,i'j'}) x_{i'j',k} x_{ij,k}}, & \text{otherwise} \end{cases} \tag{7}$$

for $i, j, i', j' = 0, 1$.

The fourth term of the product in Eq. (6), $p(\boldsymbol{r}_{1:K} \mid \boldsymbol{g}_{1:K})$, is the probability of observing the reads of all sampled individuals given their corresponding genotypes. Using the conditional independence from our HMM framework, as shown in Figure 1, we can decompose the probability $p(\boldsymbol{r}_{1:K} \mid \boldsymbol{g}_{1:K})$ as

$$p(\boldsymbol{r}_{1:K} \mid \boldsymbol{g}_{1:K}) = \prod_{k=1}^{K} p(\boldsymbol{r}_k \mid \boldsymbol{g}_k) = \prod_{k=1}^{K} \prod_{n=1}^{N_k} p(\boldsymbol{r}_{n,k} \mid \boldsymbol{g}_{n,k}) = \prod_{k=1}^{K} \prod_{n=1}^{N_k} \prod_{l=1}^{2} p(\boldsymbol{r}_{l,n,k} \mid g_{l,n,k}),$$

where $p(\boldsymbol{r}_{l,n,k} \mid g_{l,n,k})$ is the probability of observing the reads $\boldsymbol{r}_{l,n,k}$ of sampled individual n at locus l given its genotype $g_{l,n,k}$, known as the genotype likelihood, which is commonly available with aDNA data.

2.2.2. Adaptive particle marginal Metropolis-Hastings

Similar to He et al. (2022), we carry out our posterior computation by the PMMH algorithm (Andrieu et al., 2010) that enables us to jointly update the selection coefficients and population gamete frequency trajectories. More specifically, we estimate the marginal likelihood

$$p(\boldsymbol{r}_{1:K} \mid \boldsymbol{\vartheta}) = \int_{\Omega_{\boldsymbol{X}}^K} p(\boldsymbol{x}_{1:K} \mid \boldsymbol{\vartheta}) p(\boldsymbol{g}_{1:K} \mid \boldsymbol{x}_{1:K}) p(\boldsymbol{r}_{1:K} \mid \boldsymbol{g}_{1:K})\, d\boldsymbol{x}_{1:K}$$

through the bootstrap particle filter (Gordon et al., 1993), where we generate the particles from the Wright-Fisher SDE's in Eq. (5) by the Euler-Maruyama scheme. The product of the average weights of the set of particles at the sampling time points $\boldsymbol{t}_{1:K}$ yields an unbiased estimate of the marginal likelihood $p(\boldsymbol{r}_{1:K} \mid \boldsymbol{\vartheta})$, denoted by $\hat{p}(\boldsymbol{r}_{1:K} \mid \boldsymbol{\vartheta})$. The population gamete frequency trajectories $\boldsymbol{x}_{1:K}$ are sampled once from the final set of particles with their relevant weights.

Although the PMMH algorithm has been shown to work well in He et al. (2022), in practice, its performance depends strongly on the choice of the proposal. In this work, due to the increase in the number of selection coefficients required to be estimated, choosing an appropriate proposal to ensure computational efficiency becomes challenging. To resolve this issue, we adopt a random walk proposal with covariance matrix $\boldsymbol{\Gamma}$, denoted by $q(\cdot \mid \boldsymbol{\vartheta}; \boldsymbol{\Gamma})$, the Gaussian probability density function with mean vector $\boldsymbol{\vartheta}$ and covariance matrix $\boldsymbol{\Gamma}$, and under ideal conditions, the optimal choice of the covariance matrix $\boldsymbol{\Gamma}$ is a rescaled version of the covariance matrix of the posterior (Roberts & Rosenthal, 2001). Given that the covariance matrix of the posterior is commonly not available in advance, we adopt the adaptation strategy (Vihola, 2012) that can dynamically align the covariance matrix of the proposal with that of the posterior based on accepted samples. More specifically, we prespecify a target acceptance rate, denoted by A^*, and a step size sequence (decaying to zero), denoted $\{\eta^i\}_{i \geq 1}$, where the superscript denotes the iteration. The covariance matrix is updated by following the iteration formula

$$\boldsymbol{\Gamma}^i = \boldsymbol{\Gamma}^{i-1} + \eta^i (A^i - A^*) \frac{(\boldsymbol{\vartheta}^i - \boldsymbol{\vartheta}^{i-1})(\boldsymbol{\vartheta}^i - \boldsymbol{\vartheta}^{i-1})^\intercal}{\|\boldsymbol{\vartheta}^i - \boldsymbol{\vartheta}^{i-1}\|^2} \tag{8}$$

with the covariance matrix $\boldsymbol{\Gamma}^1$ (*e.g.*, $\boldsymbol{\Gamma}^1 = \sigma^2 \boldsymbol{I}$) and selection coefficients $\boldsymbol{\vartheta}^1 \sim p(\boldsymbol{\vartheta})$, where

$$\boldsymbol{\vartheta}^i \sim q(\boldsymbol{\vartheta} \mid \boldsymbol{\vartheta}^{i-1}; \boldsymbol{\Gamma}^{i-1})$$

and

$$A^i = \frac{p(\boldsymbol{\vartheta}^i)}{p(\boldsymbol{\vartheta}^{i-1})} \frac{\hat{p}(\boldsymbol{r}_{1:K} \mid \boldsymbol{\vartheta}^i)}{\hat{p}(\boldsymbol{r}_{1:K} \mid \boldsymbol{\vartheta}^{i-1})} \frac{q(\boldsymbol{\vartheta}^{i-1} \mid \boldsymbol{\vartheta}^i; \boldsymbol{\Gamma}^{i-1})}{q(\boldsymbol{\vartheta}^i \mid \boldsymbol{\vartheta}^{i-1}; \boldsymbol{\Gamma}^{i-1})}. \tag{9}$$

Such an adaptation strategy can also coerce the acceptance rate. In practice, the target acceptance rate is set to $A^* \in [0.234, 0.440]$, and the step size sequence is defined as $\eta^i = i^{-\gamma}$ with $\gamma \in (0.5, 1]$ (Vihola, 2012). See Luengo et al. (2020) and references therein for other adaptation strategies.

For the sake of clarity, we write down the robust adaptive version of the PMMH algorithm for our posterior computation:

Step 1: Initialise the selection coefficients $\boldsymbol{\vartheta}$ and population gamete frequency trajectories $\boldsymbol{x}_{1:K}$:

Step 1a: Draw $\boldsymbol{\vartheta}^1 \sim p(\boldsymbol{\vartheta})$.

Step 1b: Run a bootstrap particle filter with $\boldsymbol{\vartheta}^1$ to get $\hat{p}(\boldsymbol{r}_{1:K} \mid \boldsymbol{\vartheta}^1)$ and $\boldsymbol{x}^1_{1:K}$.

Step 1c: Initialise $\boldsymbol{\Gamma}^1$.

Repeat Step 2 until enough samples of the selection coefficients $\boldsymbol{\vartheta}$ and population gamete frequency trajectories $\boldsymbol{x}_{1:K}$ have been attained:

Step 2: Update the selection coefficients $\boldsymbol{\vartheta}$ and population gamete frequency trajectories $\boldsymbol{x}_{1:K}$:

Step 2a: Draw $\boldsymbol{\vartheta}^i \sim q(\boldsymbol{\vartheta} \mid \boldsymbol{\vartheta}^{i-1}; \boldsymbol{\Gamma}^{i-1})$.

Step 2b: Run a bootstrap particle filter with $\boldsymbol{\vartheta}^i$ to get $\hat{p}(\boldsymbol{r}_{1:K} \mid \boldsymbol{\vartheta}^i)$ and $\boldsymbol{x}^i_{1:K}$.

Step 2c: Update $\boldsymbol{\Gamma}^i$ through Eqs. (8) and (9).

Step 2d: Accept $\boldsymbol{\vartheta}^i$ and $\boldsymbol{x}^i_{1:K}$ with A^i and set $\boldsymbol{\vartheta}^i = \boldsymbol{\vartheta}^{i-1}$ and $\boldsymbol{x}^i_{1:K} = \boldsymbol{x}^{i-1}_{1:K}$ otherwise.

With sufficiently large samples of the selection coefficients $\boldsymbol{\vartheta}$ and population gamete frequency trajectories $\boldsymbol{x}_{1:K}$, we produce the minimum mean square error (MMSE) estimates for the selection coefficients $\boldsymbol{\vartheta}$ and population gamete frequency trajectories $\boldsymbol{x}_{1:K}$ through calculating their posterior means.

As in He et al. (2022), our procedure can allow the selection coefficients $s_{ij,i'j'}$ to change over time (piecewise constant), *e.g.*, let the selection coefficients $s_{ij,i'j'}(t) = s^-_{ij,i'j'}$ if $t < \tau$ otherwise $s_{ij,i'j'}(t) = s^+_{ij,i'j'}$, where τ is the time of an event that might change selection, *e.g.*, the times of

plant and animal domestication. The only modification required is to simulate the population gamete frequency trajectories $\boldsymbol{x}_{1:K}$ according to the Wright-Fisher diffusion with the selection coefficients $s^{-}_{ij,i'j'}$ for $t < \tau$ and $s^{+}_{ij,i'j'}$ for $t \geq \tau$, respectively. In this setup, we propose a scheme to test the hypothesis whether selection changes at time τ for each phenotypic trait, including estimating their selection differences, through computing the posterior $p(\Delta s_{ij,i'j'} \mid \boldsymbol{r}_{1:K})$ from the PMMH samples of the selection coefficients $s^{-}_{ij,i'j'}$ and $s^{+}_{ij,i'j'}$, where $\Delta s_{ij,i'j'} = s^{+}_{ij,i'j'} - s^{-}_{ij,i'j'}$ denotes the change in the selection coefficient at time τ. Note that our method can handle the case that the events that might change selection are different for different phenotypic traits (*i.e.*, the time τ could be taken to be different values for different phenotypic traits).

3. Results

In this section, we employ our approach to reanalyse the published ancient horse DNA data from earlier studies of Ludwig et al. (2009), Pruvost et al. (2011) and Wutke et al. (2016), where they sequenced 201 ancient horse samples in total ranging from a pre- to a post-domestication period for eight loci coding for horse coat colouration. In particular, we perform the inference of selection acting on the base coat colour controlled by *ASIP* and *MC1R* and the pinto coat pattern determined by *KIT13* and *KIT16*. Extensive simulation studies, supporting the accuracy of our methodology, are available in the supplement.

As Wutke et al. (2016) only provided called genotypes for each gene (including missing calls), we use the same scheme as in He et al. (2022) to convert to corresponding genotype likelihoods. More specifically, we take the genotype likelihood of the called genotype to be 1 and those of the remaining two to be 0 if the genotype is called, and otherwise, all possible (ordered) genotypes are assigned equal genotype likelihoods (normalised to sum to 1). Genotype likelihoods for each gene can be found in Table S1.

In what follows, we set the average length of a generation of the horse to be eight years and use the time-varying size of the horse population estimated by Der Sarkissian et al. (2015) (see Figure S1) with the reference population size $N_0 = 16000$ (*i.e.*, the most recent population size) like Schraiber et al. (2016) unless otherwise noted. Since the flat Dirichlet prior for the starting population gamete frequencies is more likely to produce low linkage disequilibrium, we generate the starting population gamete frequencies $\boldsymbol{x}_1$ through the following procedure:

Step 1: Draw $y_1, y_2 \sim \text{Uniform}(0, 1)$.

Step 2: Draw $D \sim \text{Uniform}(\max\{-y_1y_2, -(1-y_1)(1-y_2)\}, \min\{y_1(1-y_2), (1-y_1)y_2\})$.

Step 3: Set $\boldsymbol{x}_1 = ((1-y_1)(1-y_2) + D, (1-y_1)y_2 - D, y_1(1-y_2) - D, y_1y_2 + D)$.

Note that y_1 and y_2 denote the starting population frequencies of the mutant allele at the two loci, respectively, and D is the coefficient of linkage disequilibrium. We run our adaptive PMMH algorithm with 1000 particles and 20000 iterations, where we set the target acceptance rate to $A^* = 0.4$ and define the step size sequence as $\eta_i = i^{-2/3}$ for $i = 1, 2, \ldots, 20000$. We divide each generation into five subintervals in the Euler-Maruyama scheme. We discard a burn-in of 10000 iterations and thin the remaining iterations by keeping every fifth value.

3.1. Horse base coat colours

The horse genes *ASIP* and *MC1R* are primarily responsible for determination of base coat colours (*i.e.*, bay, black and chestnut). The *ASIP* gene is located on chromosome 22, whereas the *MC1R* gene is located on chromosome 3. At each locus, there are two allele types, labelled A and a for *ASIP* and E and e for *MC1R*, respectively, where the capital letter represents the ancestral allele and the small letter represents the mutant allele. See Table 1 for the genotype-phenotype map at *ASIP* and *MC1R* for horse base coat colours. Notice that *MC1R* is epistatic to *ASIP* (Rieder et al., 2001).

3.1.1. Wright-Fisher diffusion for ASIP and MC1R

Let us consider a horse population represented by the alleles at *ASIP* and *MC1R* evolving under selection over time, which induces four possible haplotypes AE, Ae, aE and ae, labelled haplotypes 00, 01, 01 and 11, respectively. We take the relative viabilities of the three phenotypes, *i.e.*, the bay, black and chestnut coat, to be 1, $1 + s_b$ and $1 + s_c$, respectively, where s_b is the selection coefficient of the black coat against the bay coat and s_c is the selection coefficient of the chestnut coat against the bay coat. See Table 2 for the relative viabilities of all genotypes at *ASIP* and *MC1R*.

We measure time in units of $2N_0$ generations and scale the selection coefficients $\alpha_b = 2N_0s_b$, $\alpha_c = 2N_0s_c$ and recombination rate $\rho = 4N_0r$, respectively. Let $X_{ij}(t)$ be the gamete frequency of haplotype ij at time t, which satisfies the Wright-Fisher SDE's in Eq. (5). More specifically,

the drift term $\boldsymbol{\mu}(t, \boldsymbol{x})$ can be simplified with the genotype-phenotype map shown in Table 2 as

$$\begin{aligned}
\mu_{00}(t, \boldsymbol{x}) &= -\alpha_b x_{10}(x_{00}x_{11} + x_{00}x_{1*}) - \alpha_c x_{00}x_{*1}x_{*1} - \frac{\rho}{2}(x_{00}x_{11} - x_{01}x_{10}) \\
\mu_{01}(t, \boldsymbol{x}) &= -\alpha_b x_{10}(x_{01}x_{11} + x_{01}x_{1*}) + \alpha_c x_{01}x_{*0}x_{*1} + \frac{\rho}{2}(x_{00}x_{11} - x_{01}x_{10}) \\
\mu_{10}(t, \boldsymbol{x}) &= -\alpha_b x_{10}(x_{10}x_{11} + x_{10}x_{1*} - x_{1*}) - \alpha_c x_{10}x_{*1}x_{*1} + \frac{\rho}{2}(x_{00}x_{11} - x_{01}x_{10}) \\
\mu_{11}(t, \boldsymbol{x}) &= -\alpha_b x_{10}(x_{11}x_{11} + x_{11}x_{1*} - x_{11}) + \alpha_c x_{11}x_{*0}x_{*1} - \frac{\rho}{2}(x_{00}x_{11} - x_{01}x_{10}),
\end{aligned}$$

where we take the scaled recombination rate to be $\rho = 2N_0$ since the two genes are located on separate chromosomes.

3.1.2. Selection of horse base coat colours

We use our method to test the null hypothesis that no change occurred in selection acting on base coat colours when horses became domesticated (in approximately 3500 BC) and estimate their selection intensities and changes. We restrict our study to the period from the start of the Holocene epoch (around 9700 BC) onwards and assume that the respective mutations occurred at both *ASIP* and *MC1R* before 9700 BC. Given that *ASIP* and *MC1R* are located on separate chromosomes, we generate the initial population gamete frequencies by following the procedure described above but fix the coefficient of linkage disequilibrium to zero. The resulting posteriors for the selection coefficients and underlying phenotype frequency trajectories of the population are shown in Figure 2, and their estimates as well as the 95% highest posterior density (HPD) intervals are summarised in Table S2.

Our estimate for the selection coefficient of the black coat is 0.0003 with 95% HPD interval $[-0.0047, 0.0053]$ from the beginning of the Holocene epoch and 0.0003 with 95% HPD interval $[-0.0028, 0.0036]$ after horses became domesticated. Our estimate for the change in the selection coefficient is around 0 with 95% HPD interval $[-0.0072, 0.0060]$. The posteriors for the selection coefficients s_b^- and s_b^+ and their difference Δs_b are all approximately symmetric about 0, which implies that the black coat was selectively neutral over the Holocene epoch, and no change took place in selection of the black coat from a pre- to a post-domestication period. Our estimate for the underlying frequency trajectory of the black coat illustrates that it keeps roughly constant through time, although with a slight decrease after horses were domesticated.

In the pre-domestication period, our estimate for the selection coefficient of the chestnut coat

is -0.0055 with 95% HPD interval $[-0.0162, 0.0061]$. Although the 95% HPD interval contains 0, we still find that the chestnut coat was most probably selectively deleterious (with posterior probability for negative selection being 0.818). In the post-domestication period, our estimate for the selection coefficient of the chestnut coat is 0.0136 with 95% HPD interval $[0.0090, 0.0184]$, suggesting that the chestnut coat was positively selected (with posterior probability for positive selection being 1.000). Combining our estimate for the change in the selection coefficient being 0.0191 with 95% HPD interval $[0.0051, 0.0297]$, we observe sufficient evidence to support that a positive change took place in selection of the chestnut coat when horses were domesticated. Our estimate for the underlying frequency trajectory of the chestnut coat reveals a slow fall from the beginning of the Holocene epoch and then a significant rise after horses became domesticated.

We also provide the results produced with a flat Dirichlet prior for the starting population gamete frequencies (see Figure S2 and Table S3). The results for selection acting on the black and chestnut coats are consistent with those shown in Figure 2.

3.2. Horse pinto coat patterns

The horse genes *KIT13* and *KIT16* are mainly responsible for determination of pinto coat patterns (*i.e.*, tobiano and sabino), both of which reside on chromosome 3, 4668 base pairs (bp) apart, with the average rate of recombination 10^{-8} crossover/bp (Dumont & Payseur, 2008). At each locus, there are two allele types, labelled *KM0* for the ancestral allele and *KM1* for the mutant allele at *KIT13* and *sb1* for the ancestral allele and *SB1* for the mutant allele at *KIT16*, respectively. See Table 3 for the genotype-phenotype map at *KIT13* and *KIT16* for horse pinto coat patterns. Note that the coat pattern, called solid, refers to a coat that neither tobiano nor sabino is present, and the coat pattern, called mixed, refers to a coat that is a mixture between tobiano and sabino.

3.2.1. Wright-Fisher diffusion for KIT13 and KIT16

We now consider a horse population represented by the alleles at *KIT13* and *KIT16* evolving under selection over time. Such a setup gives rise to four possible haplotypes *KM0sb1*, *KM0SB1*, *KM1sb1* and *KM1SB1*, labelled haplotypes 00, 01, 01 and 11, respectively. We take the relative viabilities of the four phenotypes, *i.e.*, the solid, tobiano, sabino and mixed coat, to be 1, $1+s_{to}$, $1+s_{sb}$ and $1+s_{mx}$, respectively, where s_{to} is the selection coefficient of the tobiano coat against

the solid coat, s_{sb} is the selection coefficient of the sabino coat against the solid coat, and s_{mx} is the selection coefficient of the mixed coat against the solid coat. See Table 4 for the relative viabilities of all genotypes at *KIT13* and *KIT16*.

We measure time in units of $2N_0$ generations and scale the selection coefficients $\alpha_{to} = 2N_0 s_{to}$, $\alpha_{sb} = 2N_0 s_{sb}$, $\alpha_{mx} = 2N_0 s_{mx}$ and recombination rate $\rho = 4N_0 r$, respectively. Let $X_{ij}(t)$ be the gamete frequency of haplotype ij at time t, which follows the Wright-Fisher SDE's in Eq. (5). In particular, the drift term $\boldsymbol{\mu}(t, \boldsymbol{x})$ can be simplified with the genotype-phenotype map shown in Table 4 as

$$\begin{aligned}
\mu_{00}(t,\boldsymbol{x}) &= -\alpha_{to}x_{00}(x_{10}(x_{00}+x_{*0})-x_{10}) - \alpha_{sb}x_{00}(x_{01}(x_{00}+x_{0*})-x_{01}) \\
&\quad - \alpha_{mx}x_{00}(2x_{01}x_{10}+x_{11}-x_{11}^2) - \frac{\rho}{2}(x_{00}x_{11}-x_{01}x_{10}) \\
\mu_{01}(t,\boldsymbol{x}) &= -\alpha_{to}x_{01}x_{10}(x_{00}+x_{*0}) - \alpha_{sb}x_{01}(x_{01}(x_{00}+x_{0*})-x_{0*}) \\
&\quad - \alpha_{mx}x_{01}((2x_{01}x_{10}+x_{11}-x_{11}^2)-x_{10}) + \frac{\rho}{2}(x_{00}x_{11}-x_{01}x_{10}) \\
\mu_{10}(t,\boldsymbol{x}) &= -\alpha_{to}x_{10}(x_{10}(x_{00}+x_{*0})-x_{*0}) - \alpha_{sb}x_{10}x_{01}(x_{00}+x_{0*}) \\
&\quad - \alpha_{mx}x_{10}((2x_{01}x_{10}+x_{11}-x_{11}^2)-x_{01}) + \frac{\rho}{2}(x_{00}x_{11}-x_{01}x_{10}) \\
\mu_{11}(t,\boldsymbol{x}) &= -\alpha_{to}x_{11}x_{10}(x_{00}+x_{*0}) - \alpha_{sb}x_{11}x_{01}(x_{00}+x_{0*}) \\
&\quad - \alpha_{mx}x_{11}((2x_{01}x_{10}+x_{11}-x_{11}^2)-(1-x_{11})) - \frac{\rho}{2}(x_{00}x_{11}-x_{01}x_{10}).
\end{aligned}$$

3.2.2. Selection of horse pinto coat patterns

We apply our method to test the null hypothesis that no change took place in selection acting on horse pinto coat patterns when the medieval period began (in around AD 400) and estimate their selection intensities and changes. We restrict our study to the period from the beginning of horse domestication (around 3500 BC) onwards and assume that the respective mutations occurred at both *KIT13* and *KIT16* before 3500 BC. To our knowledge, the mixed coat has never been found in the horse population, and we therefore fix the selection coefficient $s_{mx} = -1$ over time. The resulting posteriors for the selection coefficients and underlying phenotype frequency trajectories of the population are illustrated in Figure 3, and their estimates as well as the 95% HPD intervals are summarised in Table S4.

Our estimate for the selection coefficient of the tobiano coat is 0.0177 with 95% HPD interval $[0.0082, 0.0287]$ from the beginning of horse domestication and -0.0581 with 95% HPD interval

$[-0.1016, -0.0222]$ in the Middle Ages. Our estimates reveal sufficient evidence to support that the tobiano coat was positively selected after horses were domesticated but became negatively selected in the Middle Ages. Our estimate for the change in the selection coefficient is -0.0758 with 95% HPD interval $[-0.1284, -0.0355]$, which illustrates that a negative change took place in selection of the tobiano coat when the Middle Ages started. Our estimate for the underlying frequency trajectory of the tobiano coat indicates that the frequency of the tobiano coat grows substantially after horses were domesticated and then drops sharply during the medieval period.

Our estimate for the selection coefficient of the sabino coat is 0.0206 with 95% HPD interval $[-0.0050, 0.0517]$ before the Middle Ages, which shows compelling evidence of positive selection acting on the sabino coat (with posterior probability for positive selection being 0.945). However, we see that the frequency of the sabino coat declines slowly from the start of horse domestication until the loss of the sabino coat in approximately 120 BC (*i.e.*, the earliest time that the upper and lower bounds of the 95% HPD interval for the frequency of the sabino coat are both zero), probably resulting from that the sabino coat was somewhat out-competed by the tobiano coat under the tight linkage between *KIT13* and *KIT16*.

Note, we only present the resulting posterior for the selection coefficient s_{sb}^-. This is because our results show that the sabino coat became extinct before the medieval period (see Figure 3h). Without genetic variation data, the PMMH algorithm fails to converge in reasonable time for the selection coefficient s_{sb}^+, which however has little effect on estimation of the remaining three (see Figure S3, where we repeatedly run our procedure to estimate the selection coefficients s_{to}^-, s_{to}^+ and s_{sb}^- with different prespecified values of the selection coefficient s_{sb}^+ that are uniformly drawn from $[-1, 1]$).

We also provide the results produced with a flat Dirichlet prior for the starting population gamete frequencies (see Figure S4 and Table S5) and that we co-estimate the selection coefficient of the mixed coat (see Figure S5 and Table S6). Our estimate for the selection coefficient of the mixed coat is -0.5621 with 95% HPD interval $[-0.9645, -0.2262]$ before the Middle Ages. Such strong negative selection resulted in a quick loss of the mixed coat right after the domestication of the horse, which we can also find from our estimate for the underlying frequency trajectory of the mixed coat. The results for selection acting on the tobiano and sabino coats are consistent with those shown in Figure 3.

4. Discussion

To overcome a fundamental limitation of He et al. (2022), which did not aim to model genetic interactions, we presented a novel Bayesian approach for inferring temporally variable selection from the data on aDNA sequences with the flexibility of modelling linkage and epistasis in this work. Our method was mainly built upon the two-layer HMM framework of He et al. (2022), but we introduced a Wright-Fisher diffusion to describe the underlying evolutionary dynamics of two linked genes subject to phenotypic selection, which was modelled through the differential fitness of different phenotypic traits with a genotype-phenotype map. Such an HMM framework allows us to account for two-gene interactions and sample uncertainties resulting from the damage and fragmentation of aDNA molecules. Our posterior computation was carried out through a robust adaptive PMMH algorithm to guarantee computational efficiency. Unlike the original version of the PMMH of Andrieu et al. (2010), the adaption rule of Vihola (2012) was introduced to tune the covariance structure of the proposal to obtain a coerced acceptance rate in our procedure. Moreover, our method permits the reconstruction of the underlying population gamete frequency trajectories and offers the flexibility of modelling time-varying demographic histories.

We reanalysed the horse coat colour genes, *e.g.*, the *ASIP* and *MC1R* genes associated with base coat colours and the *KIT13* and *KIT16* genes associated with pinto coat patterns, based on the ancient horse samples from previous studies of Ludwig et al. (2009), Pruvost et al. (2011) and Wutke et al. (2016). Our findings match the earlier studies that the coat colour shift in the horse is considered as a domestic trait that was subject to early selection by humans (Hunter, 2018), *e.g.*, *ASIP* and *MC1R*, and human preferences have significantly changed over time and across cultures (Wutke et al., 2016), *e.g.*, *KIT13* and *KIT16*. Our results were validated with simulations that mimicked the ancient horse samples (see File S2, including Figures S6 and S7 and Tables S9 and S10, where simulation studies on performance evaluation can also be found).

For base coat colours, we conclude that there is not enough evidence available to reject the null hypotheses that the black coat was selectively neutral from a pre- to a post-domestication period and no change occurred in selection of the black coat when horses became domesticated. However, our results provide sufficient evidence to support that the chestnut coat was effectively neutral or experienced weak negative selection until the beginning of horse domestication and then became favoured by selection. We see strong evidence of such a positive change in selection

of the chestnut coat occurring when horse domestication started, which matches the findings in previous studies that selection for noncamouflaged coats might not have taken place until after horses were domesticated (see Larson & Fuller, 2014, and references therein).

For pinto coat patterns, we show strong evidence of positive selection acting on the tobiano and sabino coats before the Middle Ages. However, the frequency of the sabino coat continuously decreased from domestication until none was left (before the Middle Ages), probably because the sabino coat was somewhat out-competed by the tobiano coat under tight linkage. The tobiano coat became negatively selected during the Middle Ages. Our findings match the archaeological evidence and historical records that spotted horses experienced early selection by humans but the preference changed during the Middle Ages (see Wutke et al., 2016, and references therein).

To demonstrate the improvement attainable through modelling genetic interactions, we show the resulting posteriors for the *ASIP* and *MC1R* genes in Figure 4 and the *KIT13* and *KIT16* genes in Figure 5, respectively, which are produced through the method of He et al. (2022) with the same settings as adopted in our adaptive PMMH algorithm. We summarise the results for horse base coat colours and pinto coat patterns with their 95% HPD intervals in Tables S7 and S8, respectively. Moreover, additional simulation studies are left in File S3, including Figures S8 and S9 and Tables S11 and S12, to further illustrate the improvement resulting from modelling linkage and epistasis.

For base coat colours, we see from Figure 4 that the resulting posteriors for *ASIP* are similar to those shown in Figure 2, which indicate that black horses were selectively neutral over the Holocene epoch and no change occurred in selection of the black coat when horse domestication started. However, since the method of He et al. (2022) ignores epistatic interaction, some genotypes are incorrectly attributed to the black coat, which could alter the result of the inference of selection. As illustrated in Figure 4, the resulting posteriors for *MC1R* suggest that chestnut horses experienced positive selection from the start of the Holocene epoch onwards (with posterior probabilities for positive selection being 0.636 in the pre-domestication period and 1.000 in the post-domestication period, respectively). The evidence of a positive change that took place in selection of the chestnut coat when horses were domesticated is no longer sufficient (*i.e.*, the posterior probability is 0.430 for a positive change).

For pinto coat patterns, as illustrated in Figure 5, we see that tobiano horses were favoured

by selection since horse domestication started (with posterior probability for positive selection being 0.969) but became negatively selected during the Middle Ages (with posterior probability for negative selection being 0.983). We also find sufficient evidence against the null hypothesis that no change took place in selection of the tobiano coat when the medieval period started (with posterior probability for a negative change being 0.987). Our results for *KIT13* are compatible with those shown in Figure 3, but our results for *KIT16* are not. We observe from Figure 5 that sabino horses experienced negative selection from domestication until extinction that occurred during the Middle Ages (see Figure 5h), which means that a continuous decline in sabino horses from domestication onwards was as a result of negative selection. However when we take genetic linkage into account, we find from Figure 3 that sabino horses were favoured by selection before the Middle Ages, and such a decline was probably triggered by the sabino coat being somewhat out-competed by the tobiano coat.

Our extension inherits desirable features of He et al. (2022) along with their key limitation that all samples were assumed to be drawn after the mutant allele was created at both loci. Since allele age is usually unavailable, we have to restrict our inference to a certain time window, *e.g.*, from the time after which the mutant alleles at both loci have been observed in the sample or the time before which we assume that the mutant alleles at both loci have already existed in the population, which could bias the result of the inference of selection. An important consideration is that backward-in-time simulation of the Wright-Fisher diffusion (see Griffiths, 2003; Coop & Griffiths, 2004) is expected to resolve this issue. Moreover, how to extend our work to deal with the case of multiple interacting genes (Terhorst et al., 2015) and estimate selection coefficients and their timing of changes (Shim et al., 2016; Mathieson, 2020) will also be the topic of future investigation.

Acknowledgements

This work was carried out using the computational facilities of the Advanced Computing Research Centre, University of Bristol - `http://www.bristol.ac.uk/acrc/`.

References

Alves, J. M., Carneiro, M., Cheng, J. Y., de Matos, A. L., Rahman, M. M. et al. (2019). Parallel adaptation of rabbit populations to myxoma virus. *Science*, *363*, 1319–1326.

Andrieu, C., Doucet, A., & Holenstein, R. (2010). Particle Markov chain Monte Carlo methods. *Journal of the Royal Statistical Society: Series B (Statistical Methodology)*, *72*, 269–342.

Bank, C., Ewing, G. B., Ferrer-Admettla, A., Foll, M., & Jensen, J. D. (2014). Thinking too positive? Revisiting current methods of population genetic selection inference. *Trends in Genetics*, *30*, 540–546.

Bollback, J. P., York, T. L., & Nielsen, R. (2008). Estimation of $2N_e s$ from temporal allele frequency data. *Genetics*, *179*, 497–502.

Coop, G., & Griffiths, R. C. (2004). Ancestral inference on gene trees under selection. *Theoretical Population Biology*, *66*, 219–232.

Corbin, L. J., Pope, J., Sanson, J., Antczak, D. F., Miller, D. et al. (2020). An independent locus upstream of *ASIP* controls variation in the shade of the bay coat colour in horses. *Genes*, *11*, 606.

Darwin, C. (1859). *On the Origin of Species by Means of Natural Selection, or the Preservation of Favoured Races in the Struggle for Life*. London: John Murray.

Dehasque, M., Ávila-Arcos, M. C., Díez-del Molino, D., Fumagalli, M., Guschanski, K. et al. (2020). Inference of natural selection from ancient DNA. *Evolution Letters*, *4*, 94–108.

Der Sarkissian, C., Ermini, L., Schubert, M., Yang, M. A., Librado, P. et al. (2015). Evolutionary genomics and conservation of the endangered Przewalski's horse. *Current Biology*, *25*, 2577–2583.

Dumont, B. L., & Payseur, B. A. (2008). Evolution of the genomic rate of recombination in mammals. *Evolution*, *62*, 276–294.

Fages, A., Hanghøj, K., Khan, N., Gaunitz, C., Seguin-Orlando, A. et al. (2019). Tracking five millennia of horse management with extensive ancient genome time series. *Cell*, *177*, 1419–1435.

Ferrer-Admetlla, A., Leuenberger, C., Jensen, J. D., & Wegmann, D. (2016). An approximate Markov model for the Wright-Fisher diffusion and its application to time series data. *Genetics*, *203*, 831–846.

Fisher, R. A. (1922). On the dominance ratio. *Proceedings of the Royal Society of Edinburgh*, *42*, 321–341.

Gordon, N. J., Salmond, D. J., & Smith, A. F. M. (1993). Novel approach to nonlinear/non-Gaussian Bayesian state estimation. *IEE Proceedings F (Radar and Signal Processing)*, *140*, 107–113.

Griffiths, R. C. (2003). The frequency spectrum of a mutation, and its age, in a general diffusion model. *Theoretical Population Biology*, *64*, 241–251.

He, Z., Beaumont, M. A., & Yu, F. (2017). Effects of the ordering of natural selection and population regulation mechanisms on Wright-Fisher models. *G3: Genes, Genomes, Genetics*, *7*, 2095–2106.

He, Z., Beaumont, M. A., & Yu, F. (2020a). Numerical simulation of the two-locus Wright-Fisher stochastic differential equation with application to approximating transition probability densities. *bioRxiv*, (p. 213769).

He, Z., Dai, X., Beaumont, M. A., & Yu, F. (2020b). Detecting and quantifying natural selection at two linked loci from time series data of allele frequencies with forward-in-time simulations. *Genetics*, *216*, 521–541.

He, Z., Dai, X., Beaumont, M. A., & Yu, F. (2020c). Estimation of natural selection and allele age from time series allele frequency data using a novel likelihood-based approach. *Genetics*, *216*, 463–480.

He, Z., Dai, X., Lyu, W., Beaumont, M. A., & Yu, F. (2022). Estimating and testing selection and its changes from ancient DNA data. *bioRxiv*, (p. 502345).

Hunter, P. (2018). The genetics of domestication: Research into the domestication of livestock and companion animals sheds light both on their "evolution" and human history. *EMBO Reports*, *19*, 201–205.

Karlin, S., & Taylor, H. E. (1981). *A Second Course in Stochastic Processes*. New York: Academic Press.

552 Larson, G., & Fuller, D. Q. (2014). The evolution of animal domestication. *Annual Review of*
553 *Ecology, Evolution, and Systematics*, *45*, 115–136.

554 Loog, L., Thomas, M. G., Barnett, R., Allen, R., Sykes, N. et al. (2017). Inferring allele
555 frequency trajectories from ancient DNA indicates that selection on a chicken gene coincided
556 with changes in medieval husbandry practices. *Molecular Biology and Evolution*, *34*, 1981–
557 1990.

558 Ludwig, A., Pruvost, M., Reissmann, M., Benecke, N., Brockmann, G. A. et al. (2009). Coat
559 color variation at the beginning of horse domestication. *Science*, *324*, 485–485.

560 Luengo, D., Martino, L., Bugallo, M., Elvira, V., & Särkkä, S. (2020). A survey of Monte Carlo
561 methods for parameter estimation. *EURASIP Journal on Advances in Signal Processing*,
562 *2020*, 1–62.

563 Lyu, W., Dai, X., Beaumont, M. A., Yu, F., & He, Z. (2022). Inferring the timing and strength
564 of natural selection and gene migration in the evolution of chicken from ancient DNA data.
565 *Molecular Ecology Resources*, *22*, 1362–1379.

566 Malaspinas, A.-S. (2016). Methods to characterize selective sweeps using time serial samples:
567 an ancient DNA perspective. *Molecular Ecology*, *25*, 24–41.

568 Malaspinas, A.-S., Malaspinas, O., Evans, S. N., & Slatkin, M. (2012). Estimating allele age
569 and selection coefficient from time-serial data. *Genetics*, *192*, 599–607.

570 Mathieson, I. (2020). Estimating time-varying selection coefficients from time series data of
571 allele frequencies. *bioRxiv*, (p. 387761).

572 Mathieson, I., Lazaridis, I., Rohland, N., Mallick, S., Patterson, N. et al. (2015). Genome-wide
573 patterns of selection in 230 ancient Eurasians. *Nature*, *528*, 499–503.

574 Pruvost, M., Bellone, R., Benecke, N., Sandoval-Castellanos, E., Cieslak, M. et al. (2011).
575 Genotypes of predomestic horses match phenotypes painted in Paleolithic works of cave art.
576 *Proceedings of the National Academy of Sciences*, *108*, 18626–18630.

577 Rieder, S., Taourit, S., Mariat, D., Langlois, B., & Guérin, G. (2001). Mutations in the agouti

(*ASIP*), the extension (*MC1R*), and the brown (*TYRP1*) loci and their association to coat color phenotypes in horses (*Equus caballus*). *Mammalian Genome*, *12*, 450–455.

Roberts, G. O., & Rosenthal, J. S. (2001). Optimal scaling for various Metropolis-Hastings algorithms. *Statistical Science*, *16*, 351–367.

Schraiber, J. G., Evans, S. N., & Slatkin, M. (2016). Bayesian inference of natural selection from allele frequency time series. *Genetics*, *203*, 493–511.

Shim, H., Laurent, S., Matuszewski, S., Foll, M., & Jensen, J. D. (2016). Detecting and quantifying changing selection intensities from time-sampled polymorphism data. *G3: Genes, Genomes, Genetics*, *6*, 893–904.

Steinrücken, M., Bhaskar, A., & Song, Y. S. (2014). A novel spectral method for inferring general diploid selection from time series genetic data. *The Annals of Applied Statistics*, *8*, 2203–2222.

Tataru, P., Simonsen, M., Bataillon, T., & Hobolth, A. (2017). Statistical inference in the Wright-Fisher model using allele frequency data. *Systematic Biology*, *66*, e30–e46.

Terhorst, J., Schlötterer, C., & Song, Y. S. (2015). Multi-locus analysis of genomic time series data from experimental evolution. *PLoS Genetics*, *11*, e1005069.

Vihola, M. (2012). Robust adaptive Metropolis algorithm with coerced acceptance rate. *Statistics and Computing*, *22*, 997–1008.

Williamson, E. G., & Slatkin, M. (1999). Using maximum likelihood to estimate population size from temporal changes in allele frequencies. *Genetics*, *152*, 755–761.

Wright, S. (1931). Evolution in Mendelian populations. *Genetics*, *16*, 97–159.

Wutke, S., Benecke, N., Sandoval-Castellanos, E., Döhle, H.-J., Friederich, S. et al. (2016). Spotted phenotypes in horses lost attractiveness in the Middle Ages. *Scientific Reports*, *6*, 38548.

Data Accessibility Statement

The authors state that all data necessary for confirming the conclusions of the present work are represented completely within the article. Source code implementing the adaptive version of the PMMH algorithm described in this work is available at `https://github.com/zhangyi-he/WFM-2L-DiffusApprox-AdaptPMMH/`, where the standard version of the PMMH algorithm is also available.

Author Contributions

Z.H. designed the project and developed the method; Z.H., X.D. and W.L. implemented the method; X.D. and W.L. analysed the data under the supervision of Z.H., M.B. and F.Y.; Z.H. wrote the manuscript; X.D., W.L., M.B. and F.Y. reviewed the manuscript.

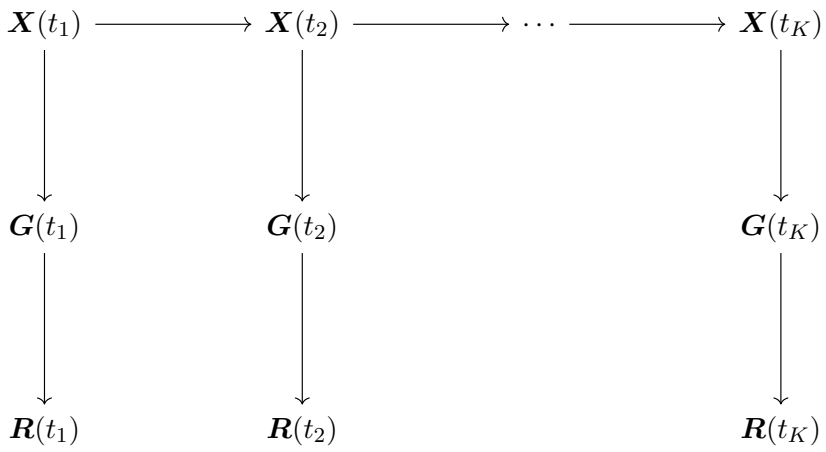

Figure 1: Graphical representation of the two-layer HMM framework extended from He et al. (2022) for the data on ancient DNA sequences.

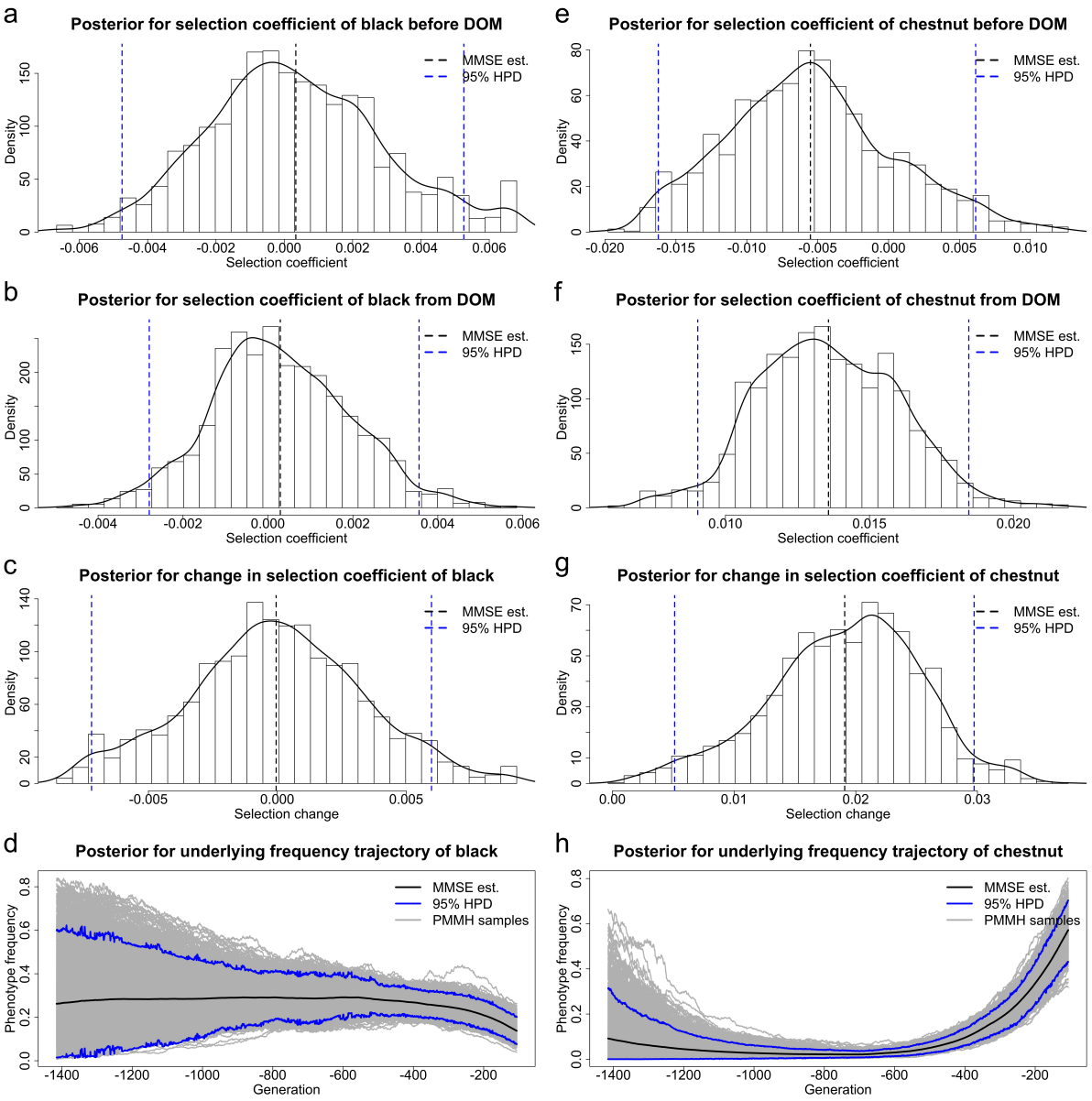

Figure 2: Posteriors for selection of horse base coat colours before and from horse domestication (starting from 3500 BC) and underlying frequency trajectories of each phenotypic trait in the population, (a)-(d) for the black coat and (e)-(h) for the chestnut coat, respectively. The samples drawn before 9700 BC, the starting time of the Holocene, are excluded. DOM stands for domestication.

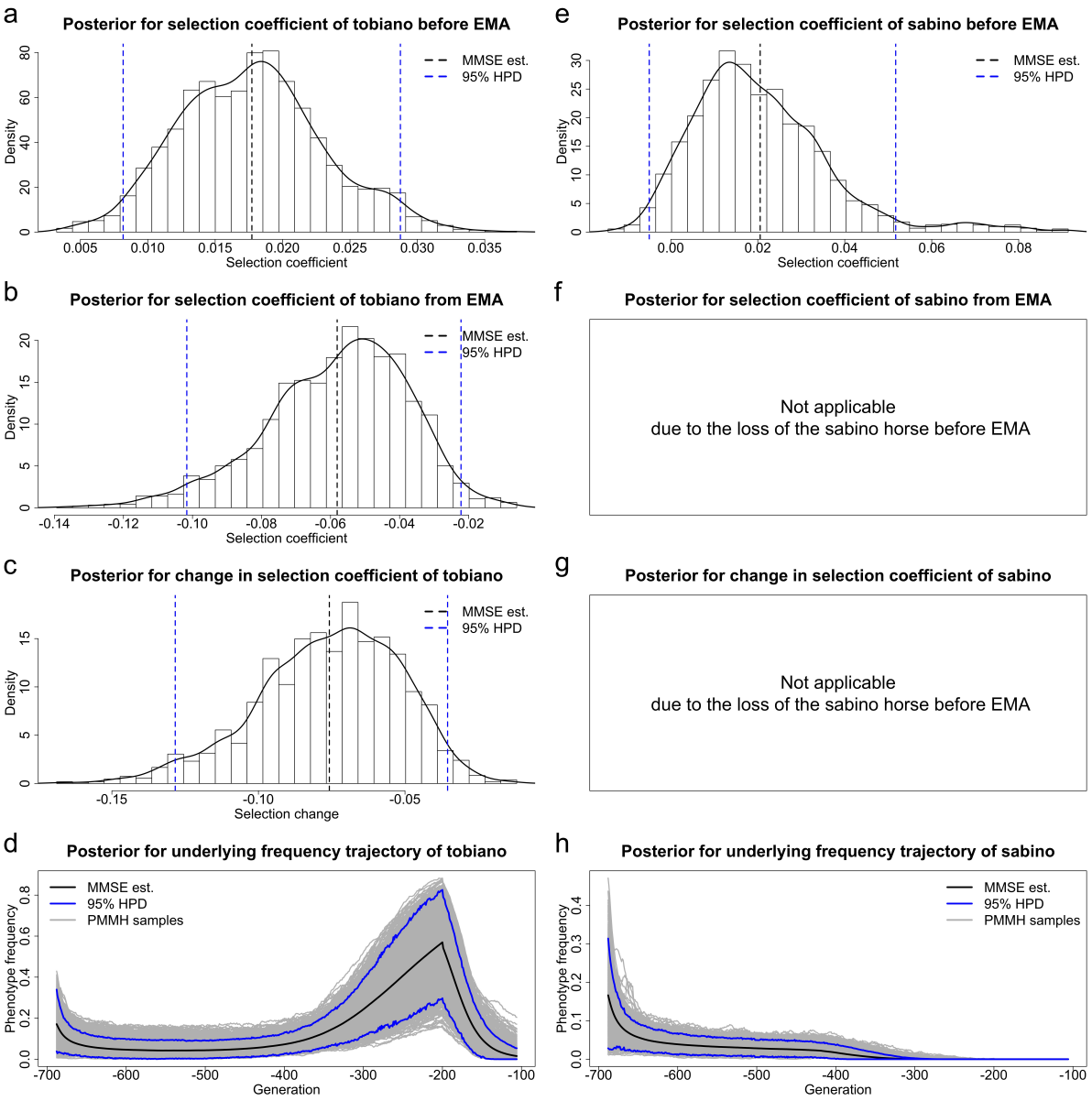

Figure 3: Posteriors for selection of horse pinto coat patterns before and from the medieval period (starting from AD 400) and underlying frequency trajectories of each phenotypic trait in the population, (a)-(d) for the tobiano coat and (e)-(h) for the sabino coat, respectively. The samples drawn before 3500 BC, the starting time of horse domestication, are excluded. EMA stands for Early Middle Ages.

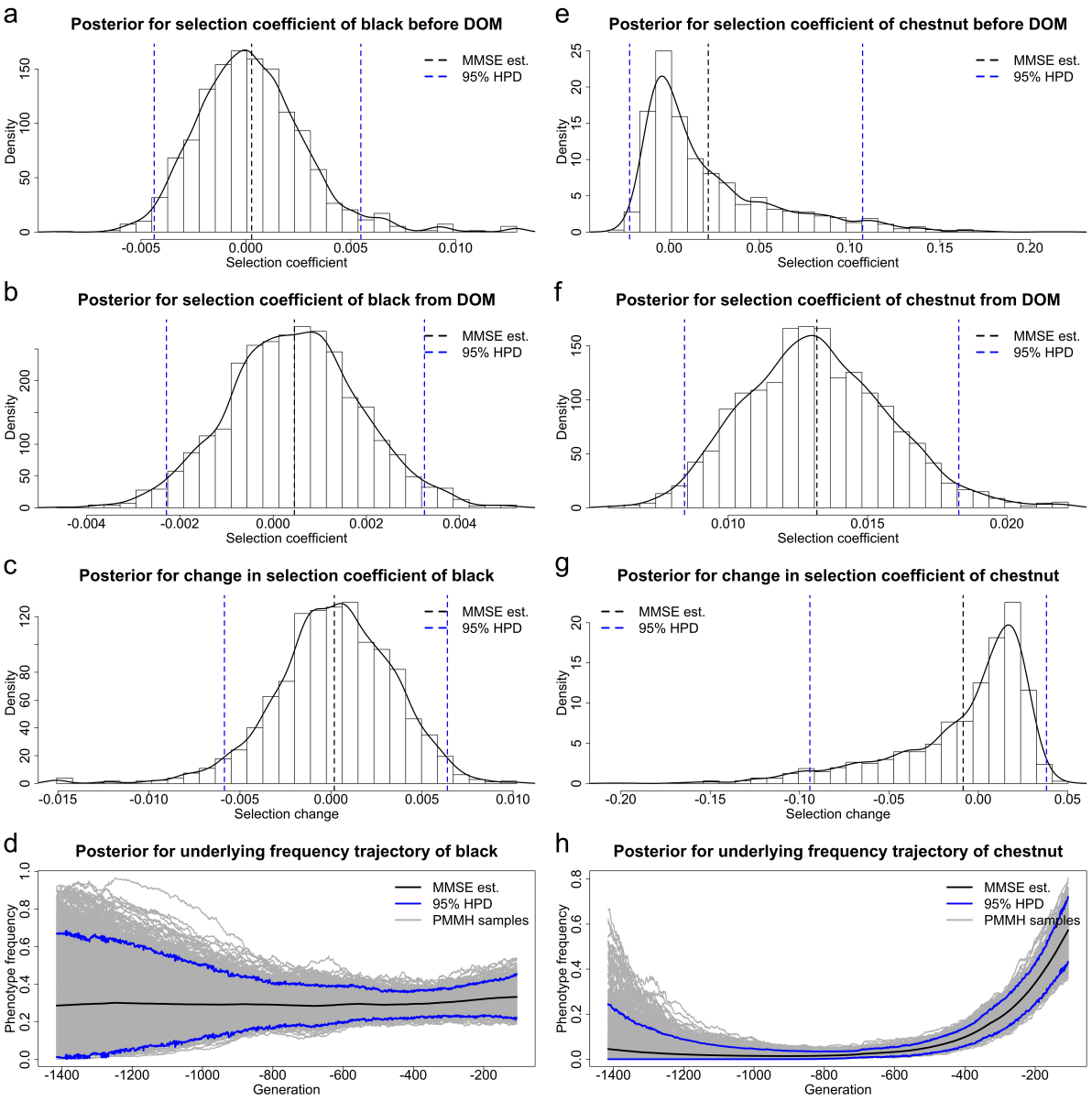

Figure 4: Posteriors for selection of horse base coat colours before and from horse domestication (starting from 3500 BC) and underlying frequency trajectories of each phenotypic trait in the population produced through the method of He et al. (2022), (a)-(d) for the black coat and (e)-(h) for the chestnut coat, respectively. The samples drawn before 9700 BC, the starting time of the Holocene, are excluded. DOM stands for domestication.

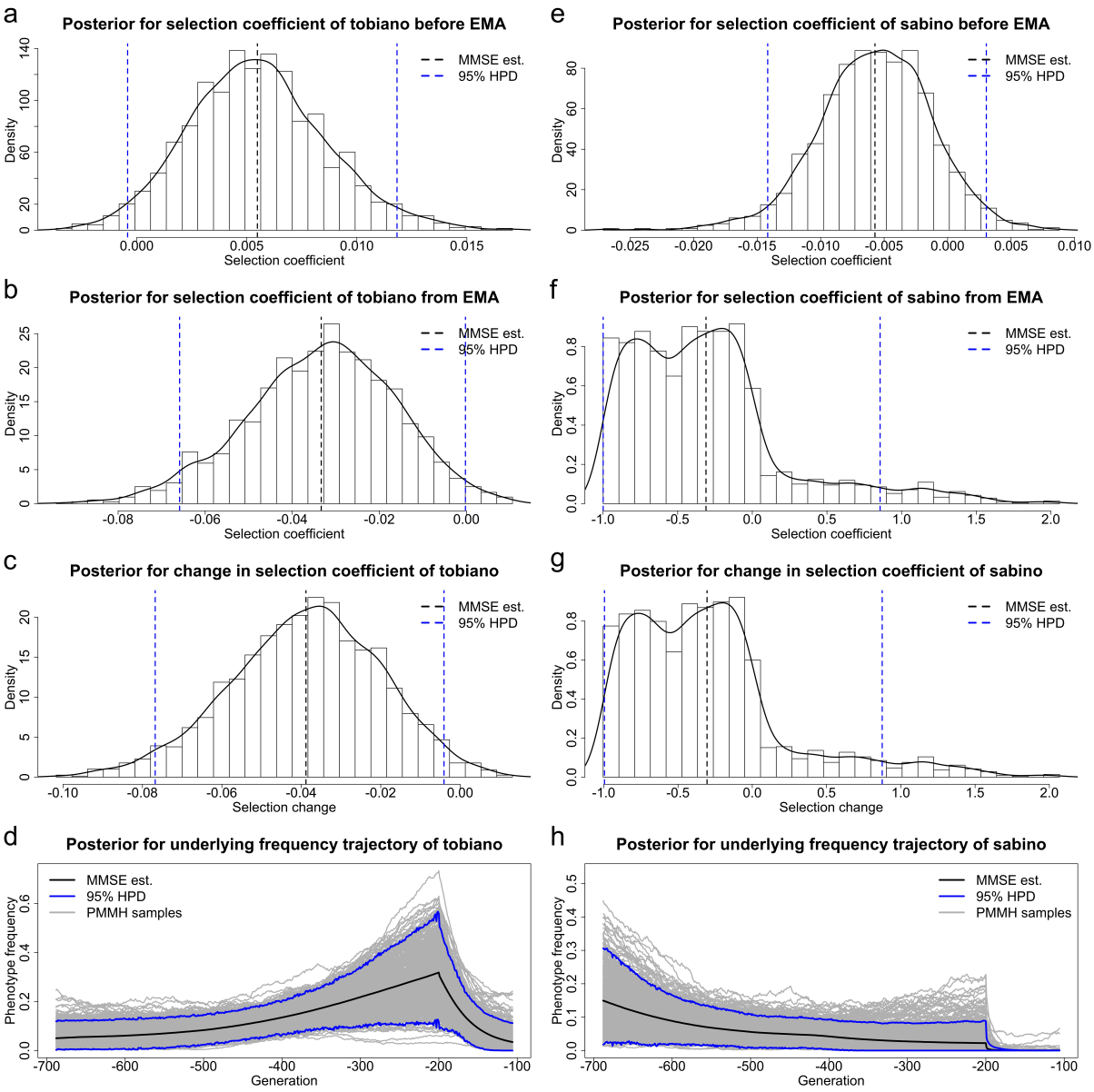

Figure 5: Posteriors for selection of horse pinto coat patterns before and from the medieval period (starting from AD 400) and underlying frequency trajectories of each phenotypic trait in the population produced through the method of He et al. (2022), (a)-(d) for the tobiano coat and (e)-(h) for the sabino coat, respectively. The samples drawn before 3500 BC, the starting time of horse domestication, are excluded. EMA stands for Early Middle Ages.

		MC1R		
		E/E	*E/e*	*e/e*
	A/A	bay	bay	chestnut
ASIP	*A/a*	bay	bay	chestnut
	a/a	black	black	chestnut

Table 1: The genotype-phenotype map at *ASIP* and *MC1R* for horse base coat colours.

	AE	Ae	aE	ae
AE	1	1	1	1
Ae	1	$1+s_c$	1	$1+s_c$
aE	1	1	$1+s_b$	$1+s_b$
ae	1	$1+s_c$	$1+s_b$	$1+s_c$

Table 2: Relative viabilities of all genotypes at *ASIP* and *MC1R*.

		KIT16		
		sb1/sb1	*sb1/SB1*	*SB1/SB1*
	KM0/KM0	solid	sabino	sabino
KIT13	*KM0/KM1*	tobiano	mixed	mixed
	KM1/KM1	tobiano	mixed	mixed

Table 3: The genotype-phenotype map at *KIT13* and *KIT16* for horse pinto coat patterns.

	KM0sb1	*KM0SB1*	*KM1sb1*	*KM1SB1*
KM0sb1	1	$1 + s_{sb}$	$1 + s_{to}$	$1 + s_{mx}$
KM0SB1	$1 + s_{sb}$	$1 + s_{sb}$	$1 + s_{mx}$	$1 + s_{mx}$
KM1sb1	$1 + s_{to}$	$1 + s_{mx}$	$1 + s_{to}$	$1 + s_{mx}$
KM1SB1	$1 + s_{mx}$	$1 + s_{mx}$	$1 + s_{mx}$	$1 + s_{mx}$

Table 4: Relative viabilities of all genotypes at *KIT13* and *KIT16*.